

Supplementary XRD data

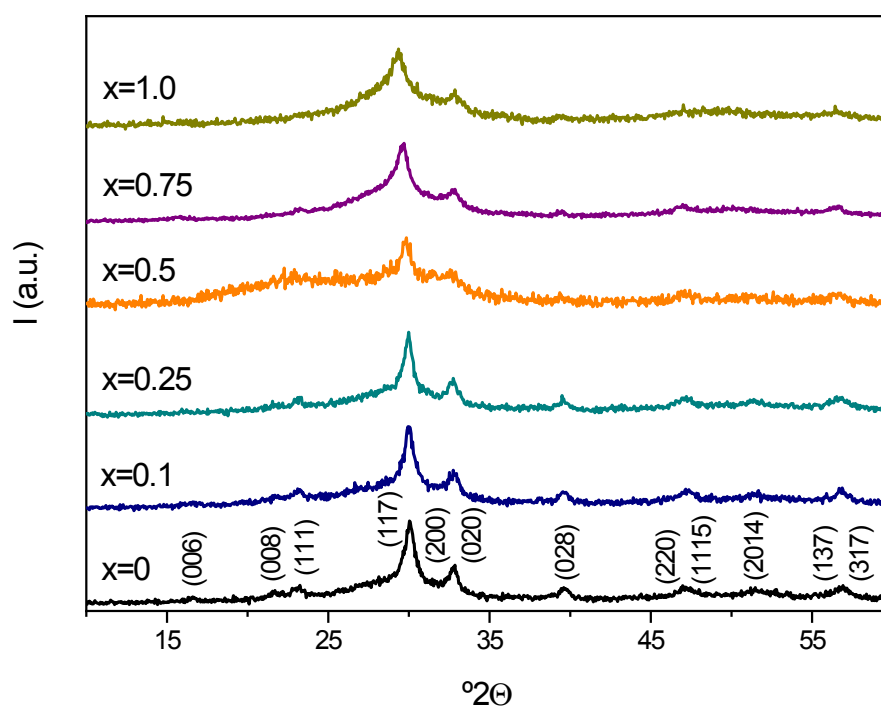


Fig. S1. XRD patterns of the Aurivillius $\text{Bi}_4\text{Ti}_{3-2x}\text{Nb}_x\text{Fe}_x\text{O}_{12}$ phases obtained by mechanosynthesis. Indexation of $\text{Bi}_4\text{Ti}_3\text{O}_{12}$ ($x=0$) as orthorhombic $B2cb$ is provided (JCPDS N. 35-0795). Neither traces of precursors nor secondary phases were found for any composition.

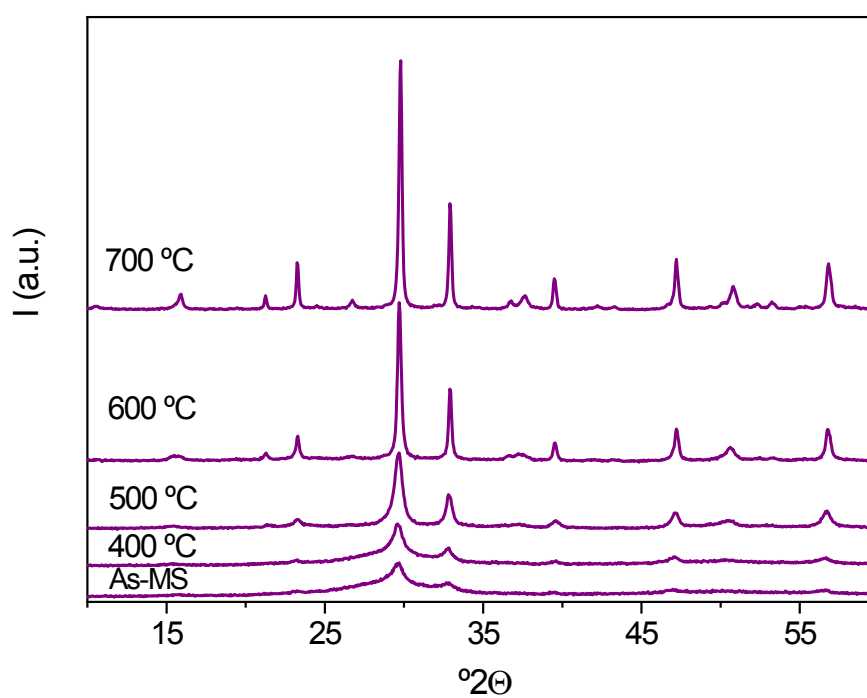


Fig. S2. XRD patterns of as-mechanosynthesized $\text{Bi}_4\text{Ti}_{1.5}\text{Nb}_{0.75}\text{Fe}_{0.75}\text{O}_{12}$ after cumulative thermal treatments at increasing temperatures. Neither residual precursors nor secondary phases appeared up to 700 °C, the limit above which this specific phase decomposes.

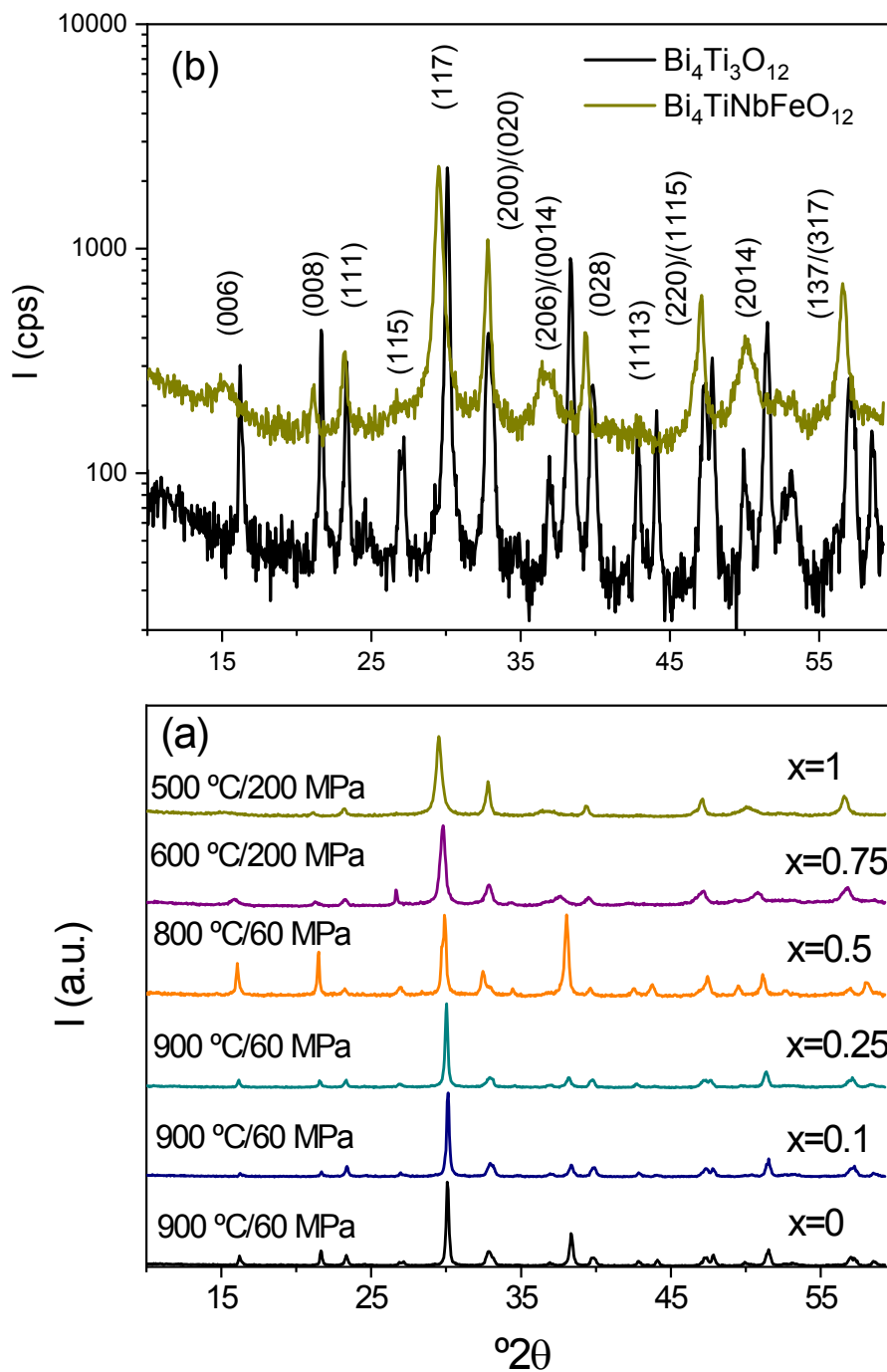


Fig. S3. (a) XRD patterns for the Aurivillius $\text{Bi}_4\text{Ti}_{3-2x}\text{Nb}_x\text{Fe}_x\text{O}_{12}$ ceramics processed by SPS of as-mechanosynthesized phases under tailored parameters. (b) Patterns for $\text{Bi}_4\text{Ti}_3\text{O}_{12}$ ($x=0$) and $\text{Bi}_4\text{TiNbFeO}_{12}$ ($x=1$) in log scale to illustrate the absence of

secondary phases for the latter material (indexation of all peaks as orthorhombic *B2cb* is provided)

Supplementary SEM data

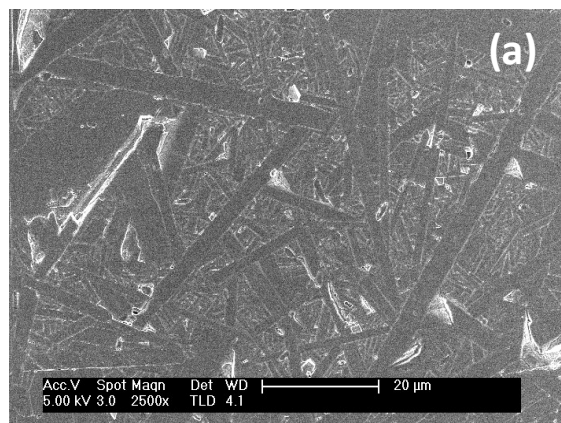
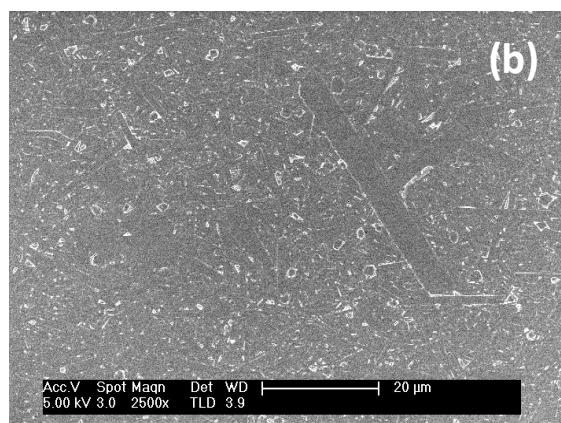
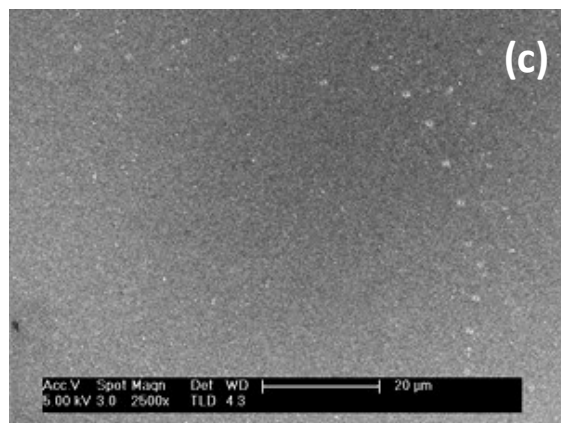


Fig. S4. Low magnification images of Aurivillius $\text{Bi}_4\text{Ti}_{3-2x}\text{Nb}_x\text{Fe}_x\text{O}_{12}$ ceramics processed by SPS of as-mechanosynthesized phases under tailored parameters: (a) $x=0$ (900 °C/60 MPa), (b) $x=0.25$ (900 °C/60 MPa), and (c) $x=0.5$ (800 °C/60 MPa). Exaggerated grain growth took place for low x -values.

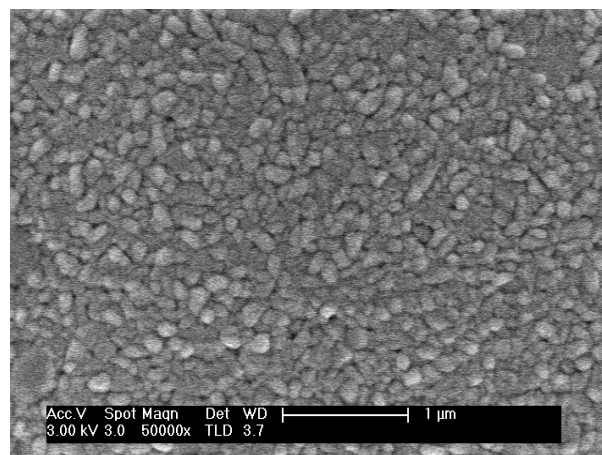
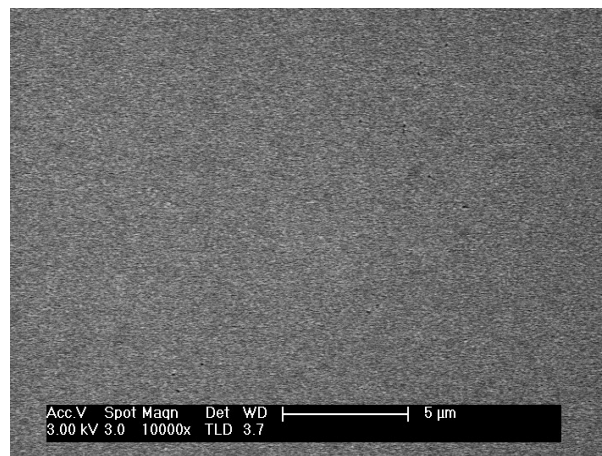
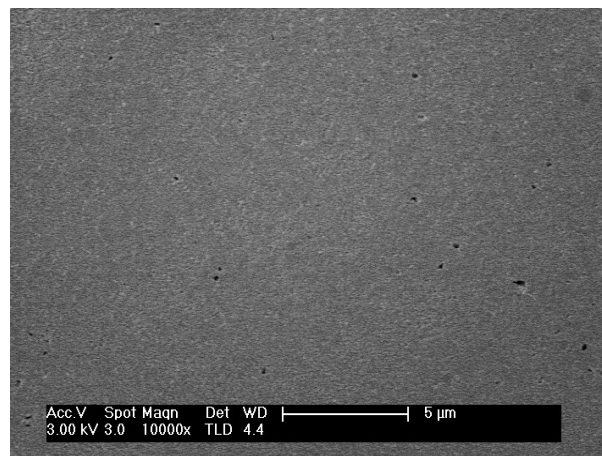


Fig S5. Reduced magnification images for the Aurivillius $\text{Bi}_4\text{TiNbFeO}_{12}$ ($x=1$) ceramic processed by SPS of as-mechanosynthesized powdered phases. Note the high microstructural homogeneity, consistently found all across the sample.

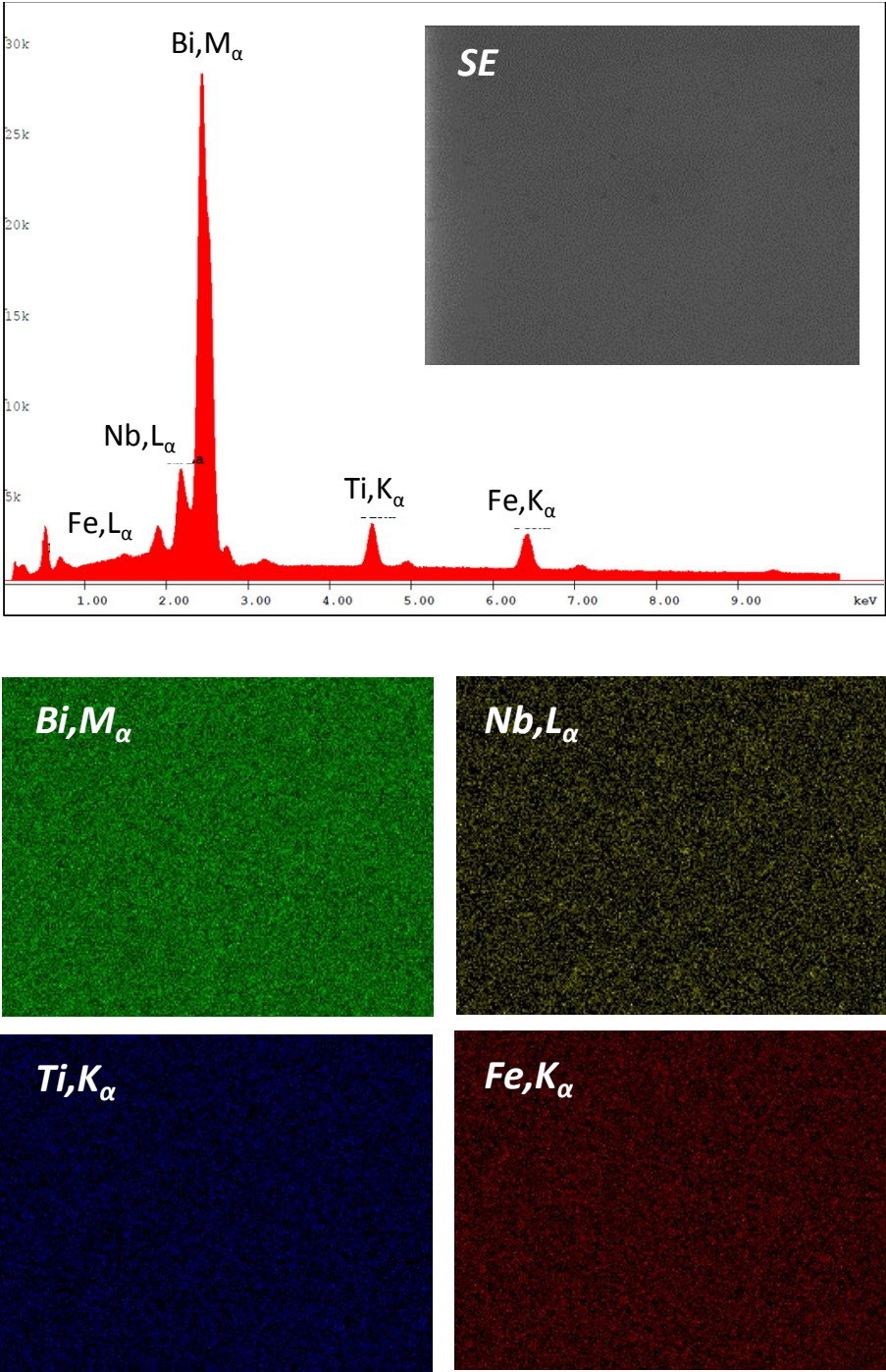


Fig S6 EDXS accumulated spectrum and elementary mapping of a 30x25 μm^2 area for the $\text{Bi}_4\text{TiNbFeO}_{12}$ ($x=1$) ceramic processed by SPS of as-mechanosynthesized powdered phases. Note the high chemical homogeneity, consistently found in mappings of variable areas

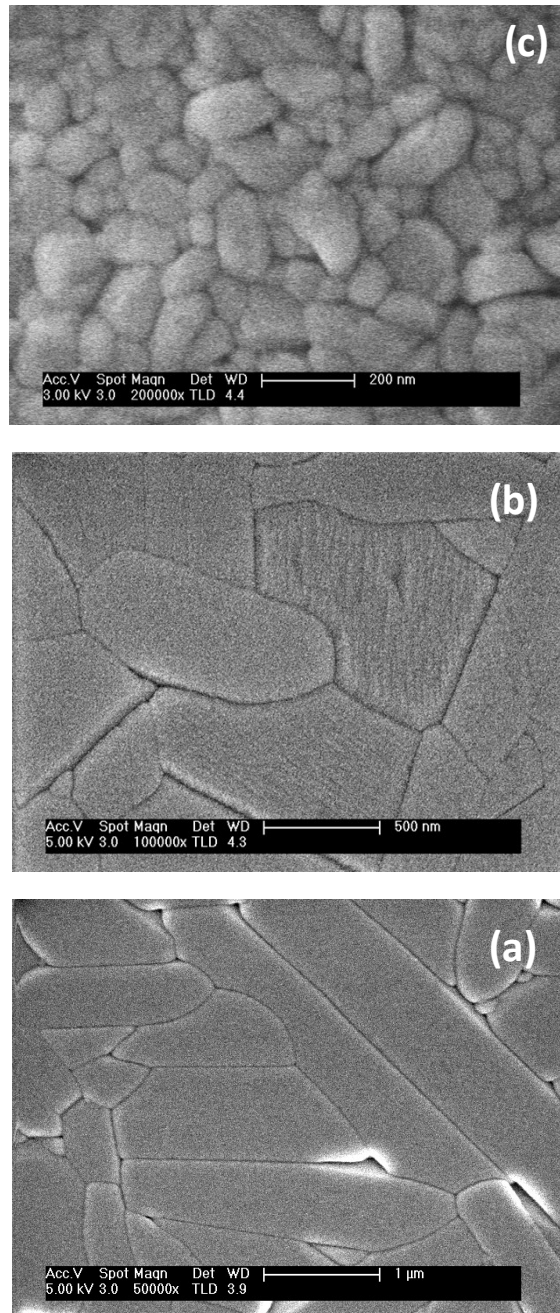


Fig. S7. Microstructure of the Aurivillius $\text{Bi}_4\text{Ti}_{3-2x}\text{Nb}_x\text{Fe}_x\text{O}_{12}$ ceramics processed by SPS of thermally treated phases of increased crystallinity, instead from as-mechanosynthesized ones: (a) $x=0.25$, (b) $x=0.5$, and (c) $x=1$. SPS conditions were

900 °C/60 MPa, 800 °C/60 MPa and 500 °C/200 MPa, respectively. To be compared with Fig. 4.

Supplementary electrical data

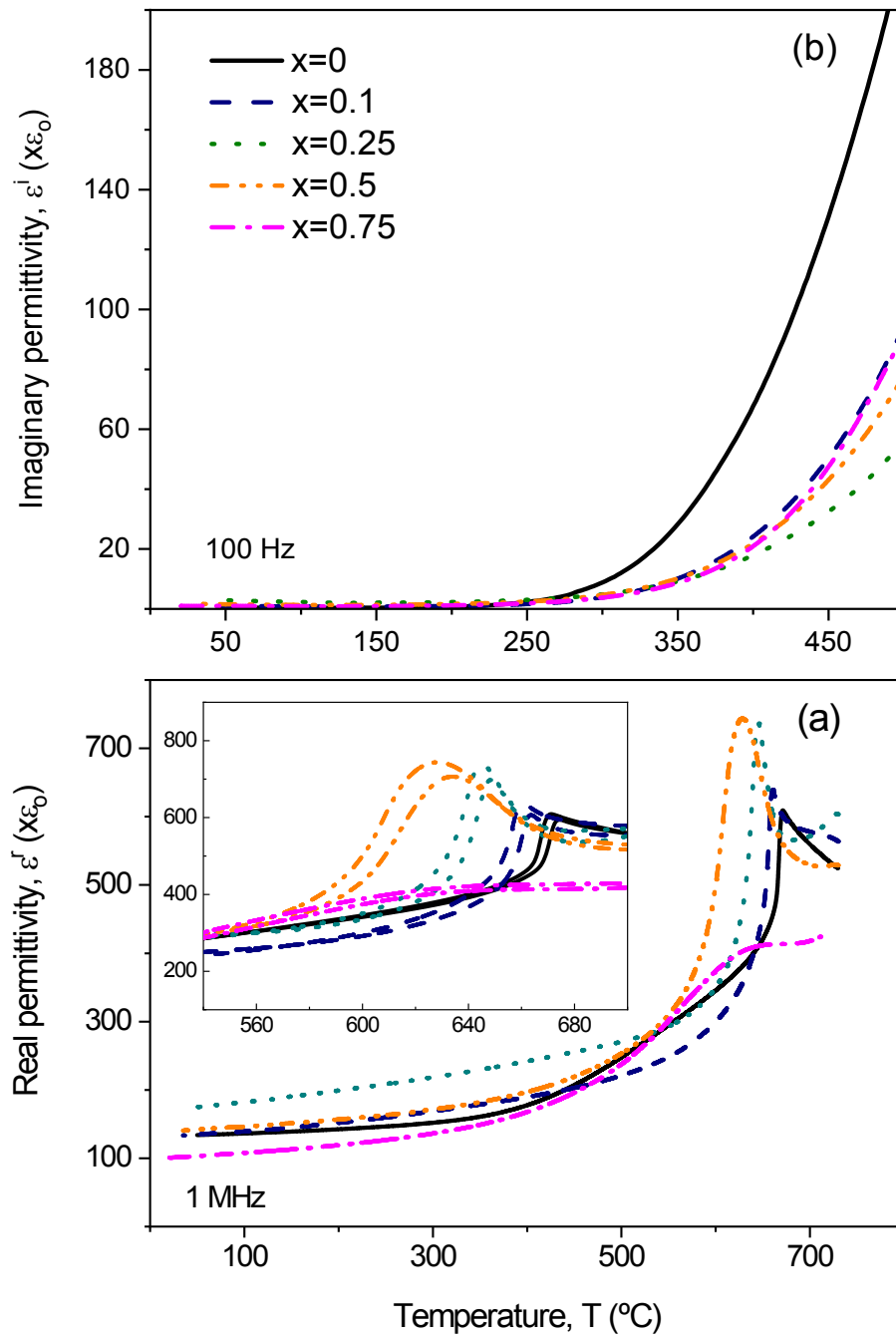


Fig. S8. Temperature dependence of the (a) real, and (b) imaginary permittivity for the $\text{Bi}_4\text{Ti}_{3-2x}\text{Nb}_x\text{Fe}_x\text{O}_{12}$ ceramics processed by SPS of thermally

treated phases, instead from as-mechanosynthesized ones, at one frequency. Inset in (a) shows the thermal hysteresis across the anomaly associated with the transition. To be compared with Fig. 7.

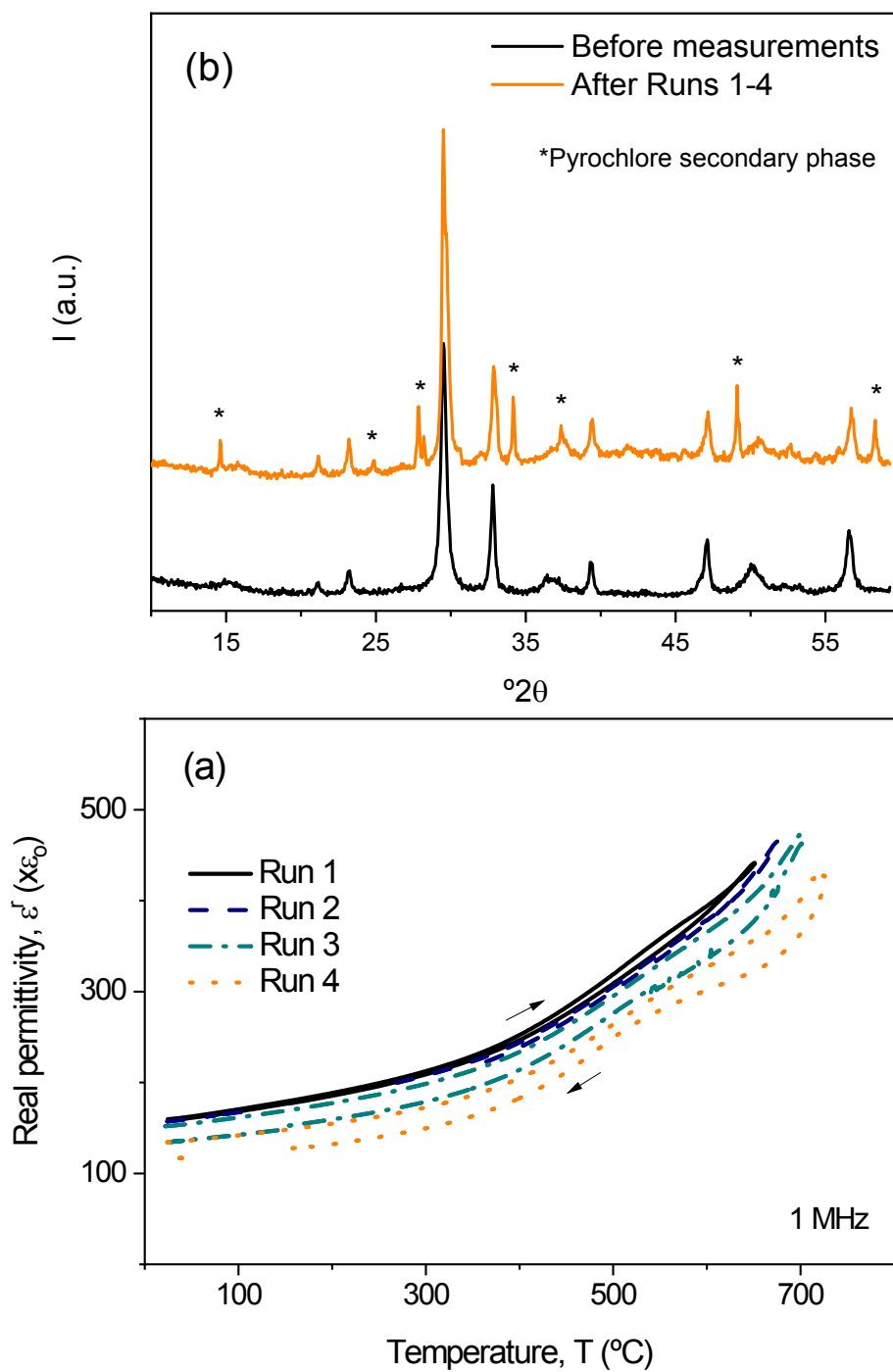


Fig. S9. (a) Evolution of the dielectric permittivity of $\text{Bi}_4\text{TiNbFeO}_{12}$ during its thermal cycling up to increasing temperatures, surpassing that of the Aurivillius oxide decomposition, (b) XRD patterns before and after the thermal cycling showing the appearance of a pyrochlore secondary phase.

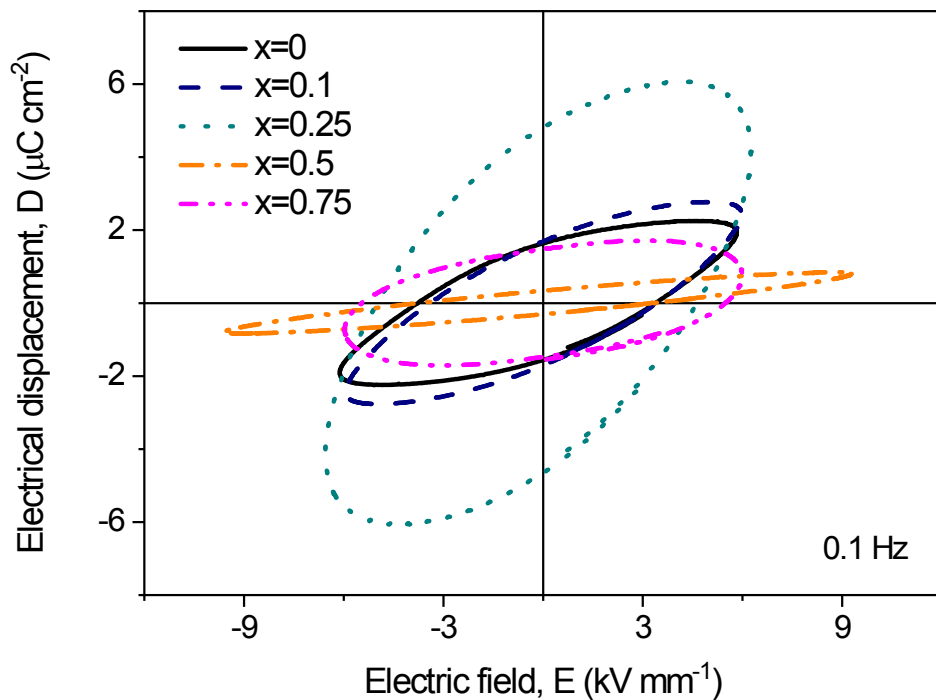


Fig. S10. RT high field electrical response for the $\text{Bi}_4\text{Ti}_{3-2x}\text{Nb}_x\text{Fe}_x\text{O}_{12}$ ceramics processed by SPS of as-mechanosynthesized nanocrystalline phases. This series of

ceramics showed reduced dielectric strength as compared with that processed from thermally treated crystalline phases. To be compared with Fig. 8(a).

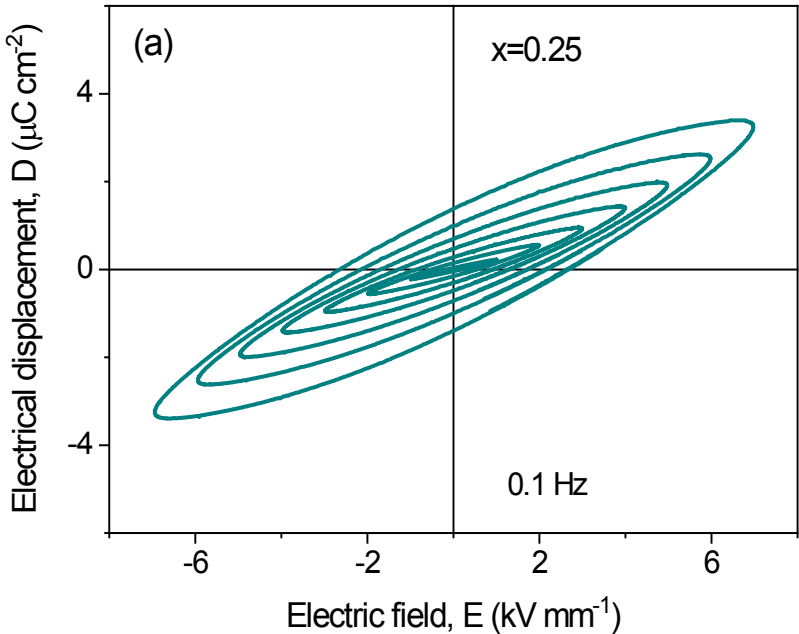
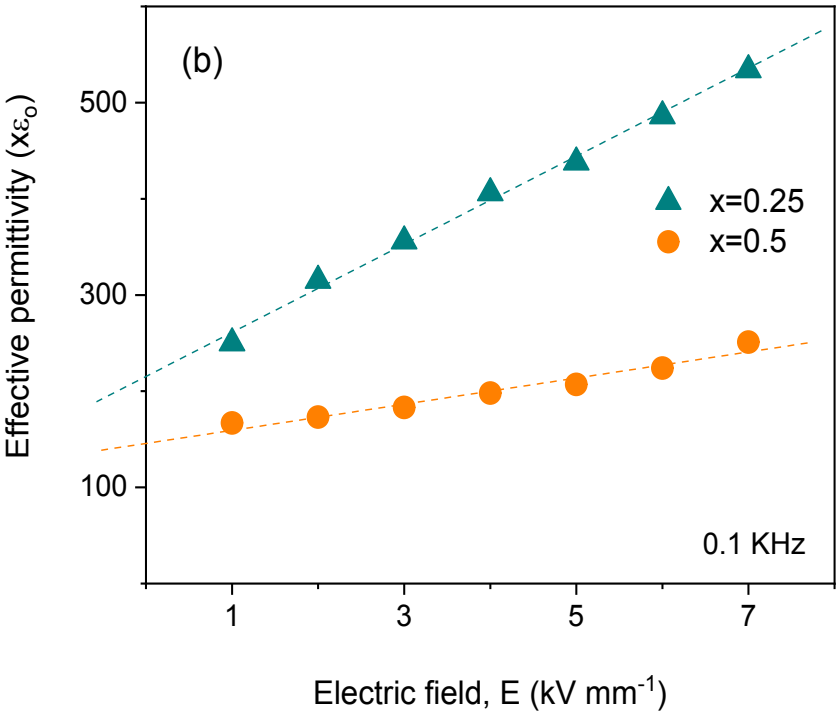


Fig. S11. (a) RT electrical response of the $\text{Bi}_4\text{Ti}_{3-2x}\text{Nb}_x\text{Fe}_x\text{O}_{12}$ ceramic processed by SPS of thermally treated crystalline phases with $x=0.25$, under increasingly high driving fields, and (b) field dependence of the effective dielectric permittivity for the ceramic materials with $x=0.25$ and 0.5 showing the presence of a Rayleigh regime, typical of ferroelectrics in the sub-coercitive range.

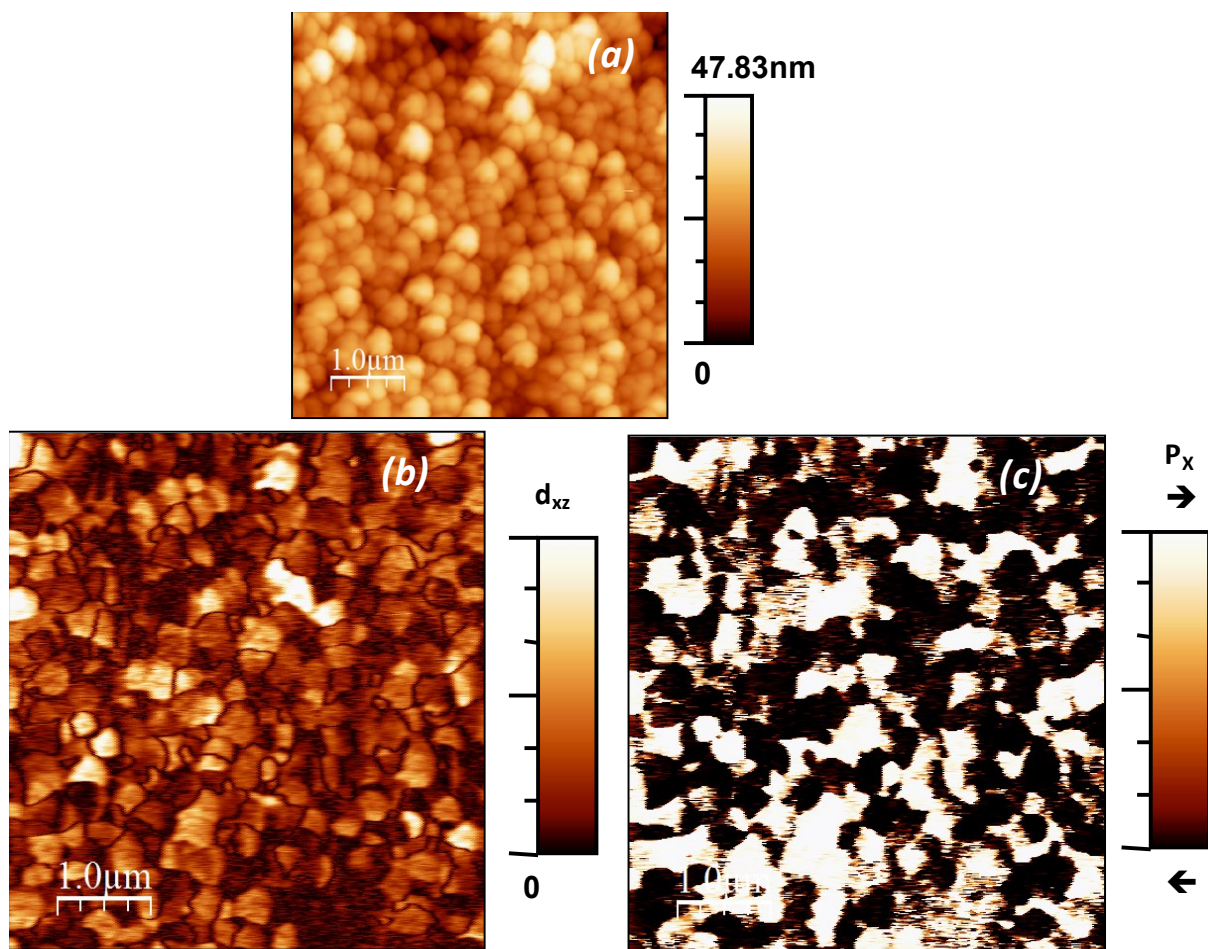


Fig. S12. (a) Topography, and piezoresponse (b) amplitude and (c) phase images of $\text{Bi}_4\text{TiNbFeO}_{12}$ demonstrating the presence of ferroelectric inversion domains.

Supplementary magnetic data

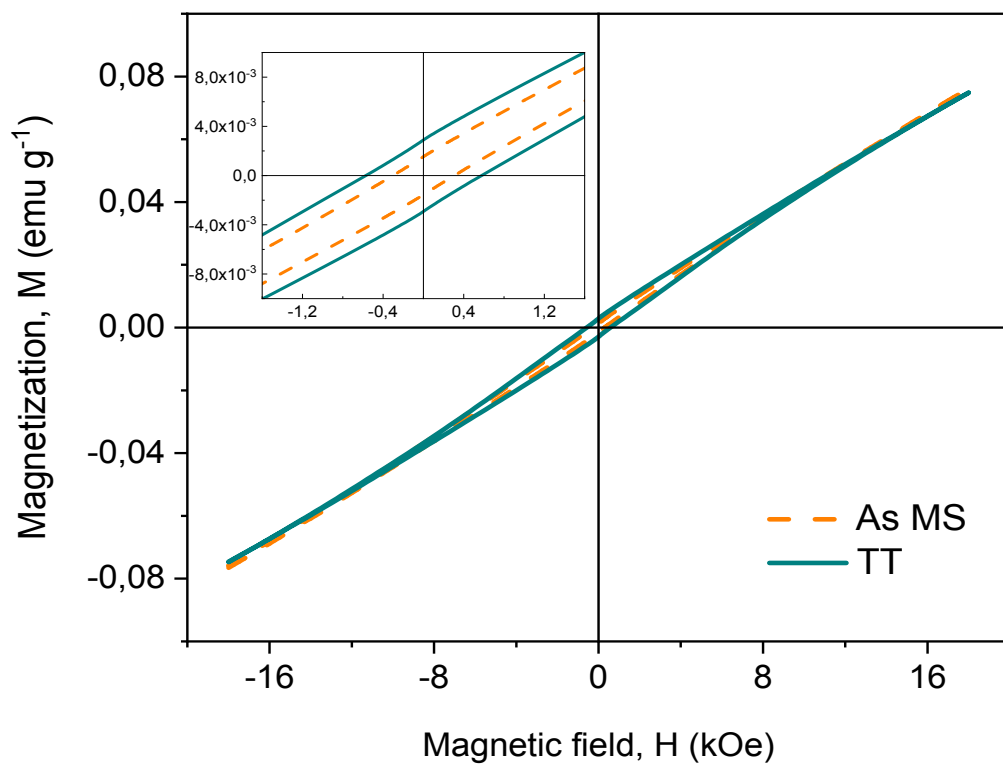


Fig. S13. RT high field magnetic response for the $Bi_4TiNbFeO_{12}$ ($x=1$) ceramic processed by SPS of as-mechanosynthesized nanocrystalline phases (As MS), compared with that for the material processed from thermally treated crystalline phases (TT). Note the reduced weak ferromagnetism.

Supplementary data for Discussion

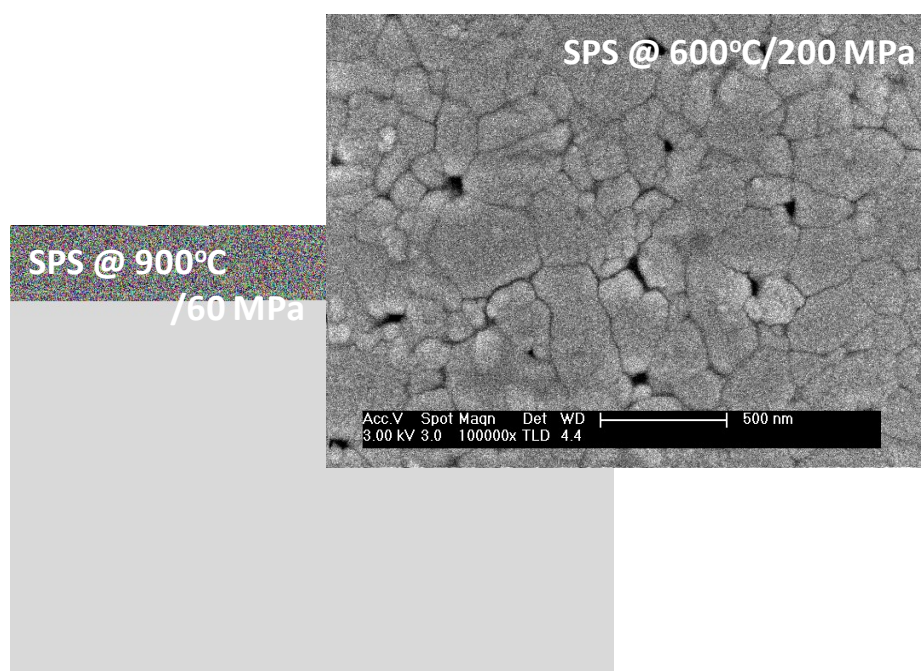
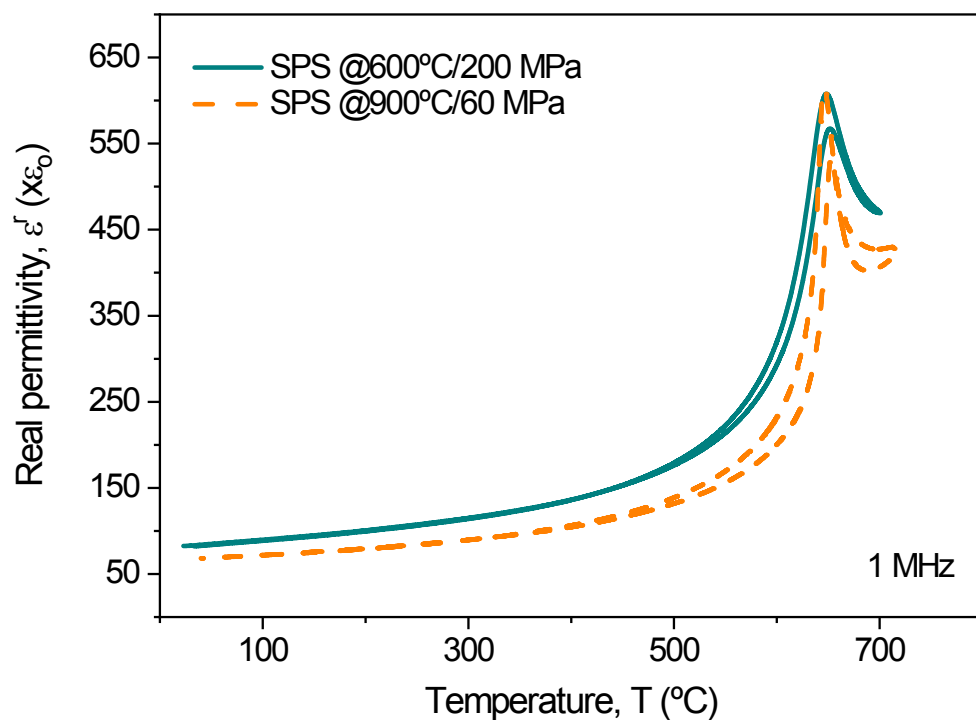


Fig. S14. Comparison of the temperature dependence of the dielectric permittivity for two $\text{Bi}_4\text{Ti}_{2.5}\text{Nb}_{0.25}\text{Fe}_{0.25}\text{O}_{12}$ ceramics with coarse and fine grained microstructures. Respective SPS conditions are indicated. No size effect on the transition diffuseness was found.